J. Fluid Mech. (1990), *vol.* 210, *pp.* 263–280
Printed in Great Britain

Buoyancy-driven fluid fracture: the effects of material toughness and of low-viscosity precursors

By JOHN R. LISTER

Research School of Earth Sciences, Australian National University, PO Box 4, Canberra 2601, ACT, Australia

(Received 3 February 1989 and in revised form 18 June 1989)

When buoyant fluid is released into the base of a crack in an elastic medium the crack will propagate upwards, driven by the buoyancy of the fluid. Viscous fluid flow in such a fissure is described by the equations of lubrication theory with the pressure given by the sum of the hydrostatic pressure of the fluid and the elastic pressures exerted by the walls of the crack. The elastic pressure and the width of the crack are further coupled by an integro-differential equation derived from the theory of infinitesimal dislocations in an elastic medium. The steady buoyancy-driven propagation of a two-dimensional fluid-filled crack through an elastic medium is analysed and the governing equations for the pressure distribution and the shape of the crack are solved numerically using a collocation technique. The fluid pressure in the tip of an opening crack is shown to be very low. Accordingly, a region of relatively inviscid vapour or exsolved volatiles in the crack tip is predicted and allowed for in the formulation of the problem. The solutions show that the asymptotic width of the crack, its rate of ascent and the general features of the flow are determined primarily by the fluid mechanics; the strength of the medium and the vapour pressure in the crack tip affect only the local structure near the advancing tip of the crack. When applied to the transport of molten rock through the Earth's lithosphere by magma-fracture, this conclusion is of fundamental importance and challenges the geophysicist's usual emphasis on the controlling influence of fracture mechanics rather than that of fluid mechanics.

1. Introduction

Molten rock, or magma, produced in the upper regions of the Earth's mantle ascends tens of kilometres through the overlying, cold and brittle lithosphere, driven by the buoyancy of the melt relative to the country rock through which it passes. It is accepted that an important mechanism for the transport of such magma is ascent through a series of fissures, or dykes, which are created by fluid-induced fracture and are held open by the fluid pressure. Evidence for this mechanism comes from field observations of the exposed remains of solidified dykes (Pollard & Muller 1976; McDonald *et al.* 1988; Reches & Fink 1988), from observations of seismic signals associated with the fracture of the country rock (Aki, Fehler & Das 1977; Shaw 1980), and from the magnitude of the ascent velocities required to explain the size and mineralogy of solid fragments carried up with the melt (Carmichael *et al.* 1977; Spera 1980).

Measurements of seismic velocities indicate that the melt initially collects in reservoirs at the base of the lithosphere. When the stress caused by the buoyancy of

the collected melt, and by any local tectonic stress, exceeds a critical value, a fissure is created in the walls of the reservoir and propagates upwards through the lithosphere, tapping the melt in the reservoir. Such a fissure may reach the Earth's surface directly, giving rise to voluminous eruptions of 'flood basalts'. More commonly (such as in Hawaii), the dyke feeds into a storage chamber of magma, located a few kilometres below the Earth's surface. Only a proportion of the magma is subsequently erupted through secondary dykes leading from the chamber to the surface. In such cases, direct measurements of the flux of magma from the mantle and of the scale of the feeder dykes are difficult. An understanding of the dynamics of magma fracture and of flow through cracks in an elastic medium is consequently of considerable importance for the correct interpretation of solidified igneous intrusions and the development of models for the long-term evolution of the Earth's crust and mantle.

Many theoretical treatments of dykes have concentrated on the calculation of the stress field around a static fluid-filled crack and on the evaluation of the conditions under which the stress intensity at the edge of the crack exceeds the critical value for the material causing the crack to extend (e.g. Weertman 1971; Pollard & Holzhausen 1979; Maaloe 1987; Rubin & Pollard 1987; Pollard 1988). In such static solutions the hydrostatic pressure in the fluid and the elastic pressure exerted by the walls of the crack are in balance. We note the result from Weertman (1971) that the vertical extent of a fluid-filled fissure cannot exceed a certain value without causing the upper tip of the crack to propagate or the lower tip to close. For geological parameters this value is of order a hundred metres and dykes of greater vertical extent will propagate upwards, the dominant pressure balance now being between the buoyancy force of the fluid and the viscous pressure drop along the dyke. This regime of dyke propagation has received much less attention and the controlling influence of the fluid dynamics has not been widely appreciated. (In contrast, a surface eruption through an *established* conduit of *given* width is usually described as a fluid-mechanical problem, e.g. Huppert *et al.* 1984.)

In this paper we present solutions for the steady propagation of a two-dimensional fluid-filled fracture driven by buoyancy in an elastic medium. This problem was considered by Spence, Sharp & Turcotte (1987) (hereinafter referred to as SST) who found a solution only for a certain value of the non-dimensional critical stress intensity of the medium and concluded that the fracture mechanics near the crack tip determined the dimensions and rate of propagation of the crack. Here, however, we exhibit a family of solutions, one solution for each value of the critical stress intensity, and conclude that the fracture mechanics determines only the local structure of the crack tip, whereas the width and rate of propagation of the crack are determined by the fluid dynamics. In these solutions the fluid pressure in the crack tip has a weak negative singularity corresponding to the viscous resistance to flow into the narrow tip (Barenblatt 1962). Since magmas contain dissolved volatiles such as water and carbon dioxide (Anderson 1978), we argue that the crack tip will be occupied by volatiles exsolved by the low pressures there and we extend our calculations to include this possibility.

The problem is formulated in §2 and the coupled equations governing the width of the crack and the fluid pressure are derived. In §3 we present asymptotic analyses for the limiting case of small volatile content. The general problem and the asymptotic analyses are solved numerically using collocation schemes described in §4. The asymptotic solutions are shown to be in agreement with limiting results from

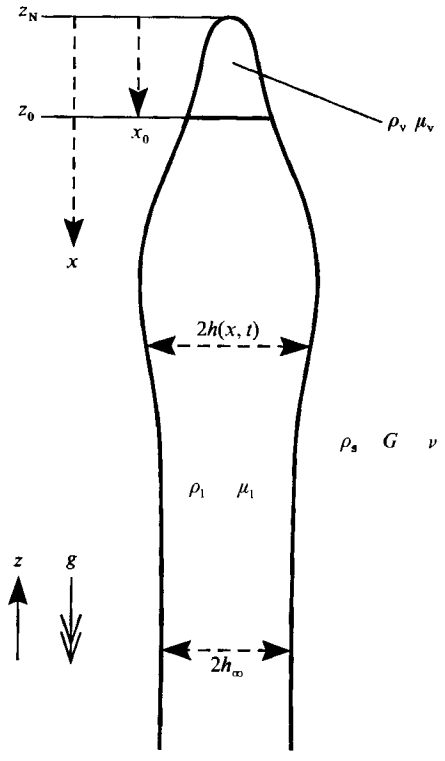

FIGURE 1. Definition sketch. A two-dimensional crack propagates vertically through an elastic solid of density ρ_s, shear modulus G and Poisson's ratio ν. The tip of the crack is occupied by vapour of density ρ_v and viscosity μ_v; the remainder is occupied by fluid of density ρ_l and viscosity μ_l. The x and z coordinate systems are as shown.

the general problem, thus providing a check on the accuracy of the numerical calculations. The results are discussed in §§5 and 6. A more detailed discussion of the geophysical implications of the results will be given in Lister (1989).

2. Formulation of the problem

Consider a two-dimensional crack propagating into a uniform elastic solid (see figure 1). Let the solid have density ρ_s, shear modulus G and Poisson's ratio ν. Let z be the vertical coordinate, $z_N(t)$ the location of the crack tip and $h(z,t)$ the half-width of the crack. Suppose that the crack is occupied by a liquid of density $\rho_l (< \rho_s)$ and viscosity μ_l in the semi-infinite region $z < z_0(t)$ and that the tip of the crack $z_0(t) < z < z_N(t)$ is occupied by vapour or gaseous volatiles of density $\rho_v (\ll \rho_l)$ and viscosity $\mu_v (\ll \mu_l)$.

The liquid flow in the crack is driven by a total effective pressure p_t derived from the body force $-\rho_l g$ on the liquid, the hydrostatic pressure $-\rho_s gz$ in the solid and the non-hydrostatic component of pressure p_e exerted by the walls of the crack due to the elastic deformation of the solid:

$$p_t = (\rho_l - \rho_s) gz + p_e + \text{const.} \tag{2.1}$$

A similar expression applies in the region occupied by vapour but with ρ_l replaced by ρ_v. Provided that $\partial h/\partial z \ll 1$ the elastic pressure is given by

$$p_e(z) = -\frac{G}{1-\nu}\frac{1}{\pi}\int_{-\infty}^{\infty}\frac{\partial h}{\partial \zeta}\frac{d\zeta}{\zeta - z} \tag{2.2}$$

(Weertman 1971). We assume that the crack is sufficiently narrow and the liquid viscosity sufficiently large that $\rho_l h^3(\partial h/\partial z)(\partial p_l/\partial z)/\mu_l^2 \ll 1$. It follows that the liquid flow satisfies the conditions of lubrication theory and, consequently, that the variations in the width of the crack are given by the horizontally averaged equation of continuity for Poiseuille flow

$$\frac{\partial h}{\partial t} = \frac{1}{3\mu_l}\frac{\partial}{\partial z}\left(h^3\frac{\partial p_l}{\partial z}\right) \quad (z < z_0). \tag{2.3}$$

Since the vapour is very much less viscous than the liquid, we may neglect density and pressure variations in the vapour and use $\rho_v \ll \rho_l$ to deduce that

$$\frac{\partial p_e}{\partial z} = \rho_s g \quad (z_0 < z < z_N). \tag{2.4}$$

We solve (2.1)–(2.4) subject to three boundary conditions. First, we assume that the liquid is injected into the crack at $z = -\infty$ at a constant rate Q. Since the elastic pressure gradient vanishes far from the crack tip, we deduce that h tends to a constant value h_∞ as $z \to -\infty$, where

$$h_\infty = \left(\frac{3\mu_l Q}{2(\rho_s - \rho_l)g}\right)^{\frac{1}{3}}. \tag{2.5}$$

Secondly, we assume that the timescale of the flow is sufficiently slow that the vapour in the crack tip is in thermodynamic equilibrium with the bulk liquid. The pressure in the vapour is equal, therefore, to the saturated vapour pressure for the fluids and the temperature concerned. In effect, this determines the location z_0 of the interface since the solutions show that if $z_N - z_0$ is too small then the pressure in the crack tip will be undersaturated and more vapour will be evaporated or exsolved until the saturated pressure is attained. Conversely, if $z_N - z_0$ is too large then vapour will condense until the saturated pressure is attained.

Thirdly, the stress immediately ahead of the crack tip must have a singularity of strength given by $-p \sim K/(2(z_N - z))^{\frac{1}{2}}$, where K is a material-dependent parameter called the critical stress-intensity factor (Irwin 1958). If the strength of the singularity were any smaller than this value then the crack would not propagate. Conversely, if the strength of the singularity were maintained at a larger value then the crack would propagate at about 40% of the speed of sound in the solid (Anderson & Grew 1977). Such propagation speeds could not be maintained by a mechanism of fracture driven by viscous flow into the crack tip. The condition on the size of the singularity in the stress may be rewritten as

$$h \sim \frac{1-\nu}{G}K(2(z_N - z))^{\frac{1}{2}} \quad (z \to z_{N-}) \tag{2.6}$$

using equation (28) of Erdelyi *et al.* (1954, p. 249).

Since the flux into the crack is constant, we seek travelling-wave solutions which propagate at some fixed speed c. We define $x = ct - z + z_N(0)$, substitute into (2.3) and

integrate once. As would be expected, we find from the boundary condition (2.5) that $c = Q/2h_\infty$. (The details of these manipulations are given by SST.) In the remaining equations we non-dimensionalize h, x, p and K with respect to the scales

$$\hat{h} = h_\infty, \quad \hat{x} = \left(\frac{Gh_\infty}{(1-\nu)(\rho_s-\rho_l)g}\right)^{\frac{1}{2}}, \quad \hat{p} = \frac{G}{1-\nu}\frac{\hat{h}}{\hat{x}}, \quad \hat{K} = \hat{p}\hat{x}^{\frac{1}{2}}. \tag{2.7}$$

From now on all quantities will be dimensionless unless stated otherwise and we shall drop the suffix on the elastic pressure defined by (2.2). We obtain

$$p(x) = -\frac{1}{\pi}\int_0^\infty \frac{h'(\xi)\,d\xi}{x-\xi}, \tag{2.8}$$

$$h \sim K(2x)^{\frac{1}{2}} \quad (x \ll 1), \tag{2.9}$$

$$p' = \frac{1}{h^2} - 1 \quad (x > x_0), \tag{2.10}$$

$$p = p_0 - Rx \quad (x \leqslant x_0), \tag{2.11}$$

where primes denote differentiation with respect to x, $R = \rho_s/(\rho_s-\rho_l)$ and $-p_0$ is the dimensionless pressure by which the hydrostatic pressure in the solid at $z = z_N$ exceeds the saturated vapour pressure. In other words, p_0 is the (negative) elastic stress which needs to be exerted by the walls of the crack for the fluid pressure in the crack tip to be decreased from the solid hydrostatic value to the saturated vapour pressure of the liquid. It is assumed that the change in p_0 as the crack propagates to shallower depths is sufficiently slow that the problem may be treated as quasi-steady and p_0 may be taken as a prescribed constant.

Equations (2.8)–(2.11) are sufficient to solve for $p(x)$, $h(x)$ and x_0 as functions of the parameters K, R and p_0. However, we first rewrite (2.8) and (2.9) in a form more suited to numerical solution. As described in SST, (2.8) may be inverted and integrated by parts to yield

$$h(x) = \frac{1}{\pi}\int_0^\infty k(\xi;x)\,p'(\xi)\,d\xi, \tag{2.12a}$$

where

$$k(\xi;x) = (x-\xi)\ln\left|\frac{x^{\frac{1}{2}}+\xi^{\frac{1}{2}}}{x^{\frac{1}{2}}-\xi^{\frac{1}{2}}}\right| - 2(x\xi)^{\frac{1}{2}}. \tag{2.12b}$$

We then use $k(\xi;x) \sim -4(x\xi)^{\frac{1}{2}}$ for $\xi \gg x$ to rewrite (2.9) as

$$\frac{\sqrt{8}}{\pi}\int_0^\infty \xi^{\frac{1}{2}}p'(\xi)\,d\xi + K = 0. \tag{2.13}$$

We note that geophysical parameters give $K \ll 1$ and so we shall include solutions for the limit $K = 0$.

A numerical scheme based on (2.10)–(2.13) will be described in §4. In this scheme it is found convenient to specify x_0 as a parameter and to calculate p_0. Solutions for a specified value of p_0 may be obtained by inverting the relationship between p_0 and x_0. In the following section we derive solutions for the asymptotic limit $p_0 \gg 1$ and deduce the limiting form of $x_0(p_0)$.

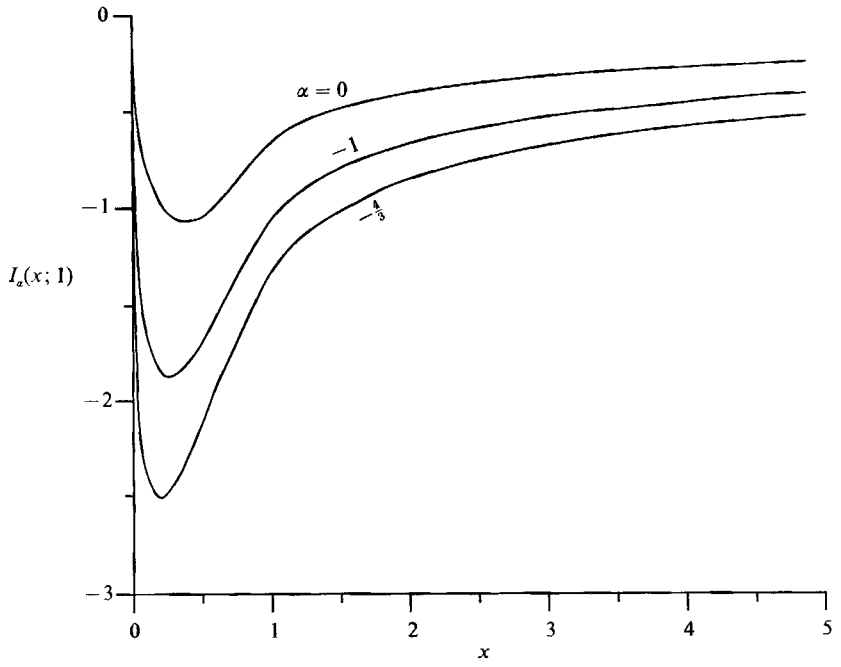

FIGURE 2. The integrals I_α (defined by (A 1) of the appendix) for $\alpha = -\frac{4}{3}$, 1 and 0. The perturbation Δh_1 of the crack width due to the pressure gradient $-\tilde{p}'$ in $x < x_0$ is given by $(\frac{4}{243})^{\frac{1}{3}} x^{\frac{2}{3}}_0 I_{-\frac{4}{3}}(x/x_0; 1)$ for $K = 0$ and by $(x_0/2K^2) I_{-1}(x/x_0; 1)$ for $K \neq 0$. The integral I_0 arises later in (4.5) during the formulation of the numerical scheme.

3. The limit $p_0 \gg 1$

If $p_0 = -\infty$ then vapour cannot be exsolved and consequently $x_0 = 0$. When $K \neq 0$ we deduce from (2.9) and (2.10) that $p \sim \ln x/2K^2$ as $x \to 0$. When $K = 0$ we deduce from (2.8), (2.10) and equation (28) of Erdelyi *et al.* (1954, p. 249) that $h \sim (\frac{243}{4})^{\frac{1}{6}} x^{\frac{2}{3}}$ and $p \sim -(\frac{4}{9})^{\frac{1}{3}} x^{-\frac{1}{3}}$ as $x \to 0$. (Such singularities were also observed by Spence & Sharp 1985 for the propagation of non-buoyant cracks since they arise from a dominant balance in the crack tip between elastic and viscous forces.) For both $K = 0$ and $K \neq 0$ there is a region of large negative pressure in the neighbourhood of $x = 0$. We expect, therefore, that if p_0 is finite then vapour will be exsolved in this neighbourhood under the influence of the low pressures. In the limit $p_0 \gg 1$ vapour is exsolved only in this neighbourhood and so the limit corresponds to $x_0 \ll 1$. Thus we seek solutions which are small perturbations Δp and Δh to the solutions $\tilde{p}$ and $\tilde{h}$ for $x_0 = 0$.

It is convenient to let $\Delta p = \Delta p_1 + \Delta p_2$ where $\Delta p_2' = 0$ in $x < x_0$ and $\Delta p_1 = 0$ in $x > x_0$. Let Δh_1 and Δh_2 be the elastic displacements due to Δp_1 and Δp_2. From the asymptotic form of $\tilde{p}$ we see that $\tilde{p}' \gg R$ in $x < x_0$. We deduce from (2.11) that $\Delta p_1' \sim -\tilde{p}'$ and calculate Δh_1 from the known form of $\tilde{p}'$. The details of the calculation are given in the appendix and the results are shown in figure 2. The functions Δp_2 and Δh_2 are then given by

$$\Delta p_2' = \frac{1}{(\tilde{h} + \Delta h_1 + \Delta h_2)^2} - \frac{1}{\tilde{h}^2} \quad (x > x_0), \tag{3.1a}$$

$$\frac{1}{\pi} \int_{x_0}^{\infty} k(\xi; x)\, \Delta p_2'(\xi)\, \mathrm{d}\xi = \Delta h_2, \tag{3.1b}$$

$$\int_{x_0}^{\infty} \xi^{\frac{1}{2}} \Delta p_2'(\xi)\, \mathrm{d}\xi = \int_0^{x_0} \xi^{\frac{1}{2}} \tilde{p}'(\xi)\, \mathrm{d}\xi. \tag{3.1c}$$

If $K \neq 0$ then $\Delta h_1 \ll \tilde{h}$ everywhere (see figure 2). Equation (3.1*c*) suggests that Δp_2, and hence Δh_2, are $O(x_0^{\frac{1}{3}})$. Thus $\Delta h_1 \ll \Delta h_2 \ll \tilde{h}$ except near $x = x_0$. Since the integrals on the left-hand sides of (3.1*b*) and (3.1*c*) are dominated by the contributions from $x \gg x_0$, we may replace their lower limits by zero, neglect Δh_1 in (3.1*a*) and linearize with respect to Δh_2. After defining $\Delta h_2 = x_0^{\frac{1}{3}}\phi(x)$ and $\Delta p_2 = x_0^{\frac{1}{3}}\psi(x)$, we obtain

$$\psi' = -\frac{2\phi}{\tilde{h}^3}, \tag{3.2a}$$

$$\frac{1}{\pi}\int_0^\infty k(\xi;x)\,\psi'(\xi)\,\mathrm{d}\xi = \phi, \tag{3.2b}$$

$$\int_0^\infty \xi^{\frac{1}{3}}\psi'(\xi)\,\mathrm{d}\xi = \frac{1}{K^2}. \tag{3.2c}$$

If $K = 0$ then $\Delta h_1 \geqslant O(\tilde{h})$ in $x \leqslant O(x_0)$. From (3.1*a*) we infer large values of Δp_2 in this region. The appropriate scalings may be shown to be $\Delta p_2' = (\frac{4}{243})^{\frac{1}{3}} x_0^{-\frac{4}{3}}\psi'(s)$ and $\Delta h_2 = (\frac{243}{4})^{\frac{1}{6}} x_0^{\frac{2}{3}}\phi_2(s)$, where $s = x/x_0$. We use the asymptotic forms of $\tilde{p}$ and $\tilde{h}$ and write $\Delta h_1 = (\frac{243}{4})^{\frac{1}{6}} x_0^{\frac{2}{3}}\phi_1(s)$ to obtain

$$\psi' = \frac{1}{(x^{\frac{2}{3}}+\phi_1+\phi_2)^2} - x^{-\frac{4}{3}} \quad (x > 1), \tag{3.3a}$$

$$\frac{1}{\pi}\int_1^\infty k(\xi;x)\,\psi'(\xi)\,\mathrm{d}\xi = \phi_2, \tag{3.3b}$$

$$\int_1^\infty \xi^{\frac{1}{3}}\psi'(\xi)\,\mathrm{d}\xi = 6. \tag{3.3c}$$

Numerical solutions of (3.2) and (3.3) will be presented in §5 and compared with limiting solutions of (2.10)–(2.13). We note here that the perturbations due to a small volume of vapour are different in form for $K \neq 0$ and $K = 0$: for $K \neq 0$ the perturbation is much smaller than $\tilde{h}$ but extends over an $O(1)$ region; for $K = 0$ the perturbation is $O(\tilde{h})$ but extends over a very small region. The asymptotic relationships between p_0 and x_0 as $x_0 \to 0$ are

$$p_0 \sim \tilde{p}(x_0) \sim \frac{1}{2K^2}\ln x_0 + c \quad (K \neq 0), \tag{3.4}$$

where c is a constant given by the behaviour of $\tilde{p}$ for each K, and

$$p_0 \sim \tilde{p}(x_0) + \Delta p_2(x_0) \sim -\left(\frac{4}{243x_0}\right)^{\frac{1}{3}}(3+\psi(1)) \quad (K = 0). \tag{3.5}$$

4. The numerical scheme

We wish to solve (2.10)–(2.13) numerically. As indicated earlier, we will take x_0 as a given parameter and p_0 as a quantity to calculate. We first make the substitution $x = \tan^2 y, \xi = \tan^2\eta$ in order to remove the square-root singularities in the integrands of (2.12*a*) and (2.13) and to transform the range of integration onto the finite interval $(0, \frac{1}{2}\pi)$. From (2.9) and (2.10) we see that $p' \sim 1/2K^2x$ as $x \to 0$ when $x_0 = 0$ and $K \neq 0$. Further, by writing (2.8) as

$$p = \frac{1}{\pi x}\int_0^\infty h'(\xi)\,\mathrm{d}\xi - \frac{1}{\pi x}\int_0^\infty \frac{\xi h'(\xi)\,\mathrm{d}\xi}{x-\xi} = \frac{1}{\pi x} + O\left(\frac{1}{x^2}\right) \tag{4.1}$$

we see that $p' \sim -1/\pi x^2$ as $x \to \infty$. (Higher-order terms are derived by SST.) These limiting forms for p' suggest making the substitution $f = p'x(x+1)$. In terms of the new variables

$$h(y) = \int_0^{\frac{\pi}{2}} \mathscr{K}(\eta; y) f(\eta)\, \mathrm{d}\eta, \tag{4.2}$$

$$\frac{\sqrt{32}}{\pi} \int_0^{\frac{\pi}{2}} f(\eta)\, \mathrm{d}\eta + K = 0, \tag{4.3}$$

$$p(y) = 2 \int_y^{\frac{\pi}{2}} f(\eta) \cot \eta\, \mathrm{d}\eta, \tag{4.4}$$

where $\mathscr{K}(\eta; y) = (2 \cot \eta/\pi)\, k(\tan^2 \eta; \tan^2 y)$. The unknowns f and h are smooth polynomic functions of y except when $K = 0$ and $x_0 = 0$ in which case $f \sim y^{-\frac{2}{3}}$ and $h \sim y^{\frac{4}{3}}$ as $y \to 0$.

SST approximated f by a cosine series

$$f = \sum_{i=0}^{n} a_i \cos(2iy),$$

which allowed them to evaluate the right-hand side of (4.2) analytically. They considered only $K \neq 0$ and $x_0 = 0$ for which case it may be shown that the error in the approximation is $O(n^{-2})$ (Carslaw 1930). However, the cosine representation leads to a number of difficulties: if $K = 0$ and $x_0 = 0$ then the singularity in f causes the error to deteriorate to $O(n^{-\frac{1}{3}})$; if $x_0 \neq 0$ then it is difficult to apply (2.11); and if the approximation is used only in the interval $x \geqslant x_0 > 0$ then (4.2) can no longer be evaluated analytically.

We choose, instead, to approximate f by a piecewise-linear function defined by the values $f_i \equiv f(x_i)$ of f at $n+1$ evenly spaced points $y_0 = \tan^{-1} x_0^{\frac{1}{2}}, y_1, \ldots, y_n = \frac{1}{2}\pi$. For the special case $x_0 = 0$, $K = 0$ we approximate $g \equiv f\eta^{\frac{2}{3}}$ by a piecewise-linear function defined by values g_i. The error in the approximation is $O(n^{-2})$ and we note that it would be easy to generalize the method to use a cubic-spline approximation with error $O(n^{-4})$.

Substituting (2.10), (2.11) and the approximation for f into (4.2) we obtain

$$\frac{f}{x(x+1)} = \left\{ \sum_{i=0}^{n} f_i h_i(y) - \frac{R}{\pi} \int_0^{x_0} k(\xi; \tan^2 y)\, \mathrm{d}\xi \right\}^{-2} - 1, \tag{4.5}$$

where the $h_i(y)$ are integrals of $\mathscr{K}$ multiplied by simple functions of η and are independent of f. The integral in (4.5) is evaluated in the Appendix and the values of h_i at a given y_j may be evaluated by a simple quadrature scheme. Equations (4.3) and (4.4) reduce to linear algebraic equations in the f_i (or g_i). We determine the unknowns f_i (or g_i) by taking (4.5) evaluated at $y = y_1, \ldots, y_{n-1}$ together with (4.3). If $x_0 > 0$ we also evaluate (4.5) at $y = y_0$, if $x_0 = 0$ and $K \neq 0$ we use $f_0 = \frac{1}{2}K^2$ and if $x_0 = 0$ and $K = 0$ we use $g_0 = (\frac{4}{243})^{\frac{1}{3}}$. This set of $n+1$ equations is solved for the $n+1$ unknowns by a variant of Newton's method which incorporates step-halving to ensure that the norm of the residual error decreases. The shape of the crack, the pressure distribution and p_0 are then readily calculated.

It was found that $n = 100$ was sufficient to ensure an accuracy of one part in 10^4 in all the quantities calculated. The values of h_i were calculated numerically to within one part in 10^6. Newton's method was found to converge rapidly in at most ten or so iterations, even from quite arbitrary initial guesses. Quasi-Newton methods and

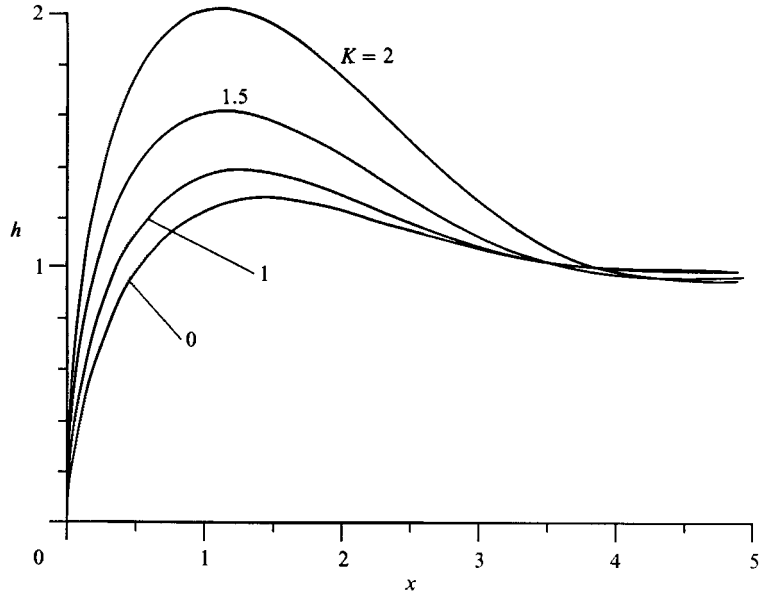

FIGURE 3. The variation of the shape of the crack with K for $x_0 = 0$.

the minimization of the norm of the residual error, though requiring less effort per iteration, were found to require many more iterations.

The numerical scheme is easily adapted for the solution of the asymptotic problems (3.2) and (3.3) since the structure of the equations and the form of the solutions are similar to those of (2.10), (2.12) and (2.13). The chief difference between the schemes lies in the use of (3.2*a*) or (3.3*a*) instead of (2.10) to derive the equations analogous to (4.5). We note from (3.2*a*, *c*) that $\psi' \sim \sqrt{8/\pi K^5 x}$ as $x \to 0$.

5. Results

The first problem to consider is that in which $x_0 = 0$ and the crack is completely occupied by fluid. Numerical solutions to (2.10), (2.12) and (2.13) were found for all values of K and some of the calculated crack profiles are shown in figure 3. Each profile exhibits a bulbous nose at $x \approx 1$ and a slight neck at $x \approx 5$ and rapidly asymptotes to $h = 1$ as $x \to \infty$. The size $h_{\max}$ and location $x_{\max}$ of the maximum width of the crack are shown as functions of K in figures 4 and 5. The insensitivity of these quantities to changes in K when $K \ll 1$ reflects the fact that such changes are accommodated by local perturbations to h in $x \ll 1$ and, consequently, the shape near $x = x_{\max}$ is unaltered (cf. derivation of (3.3)).

The existence of solutions for all values of K contrasts with the results of SST who found a solution only for $K \approx 1.84955$. Solutions for all values of K were obtained, however, for the related problem of fluid fracture in the absence of buoyancy (Spence & Sharp 1985). In the calculations of buoyancy-driven fracture by SST a cosine-series approximation to f was used, h was calculated from (4.2) and an objective function F was defined to be the sum of the squared errors in (2.10) evaluated at M sample values of x. The objective F was minimized as a function of the first N coefficients of the cosine series, where $N < M$, and K was calculated from the resulting solution rather than being imposed upon it.

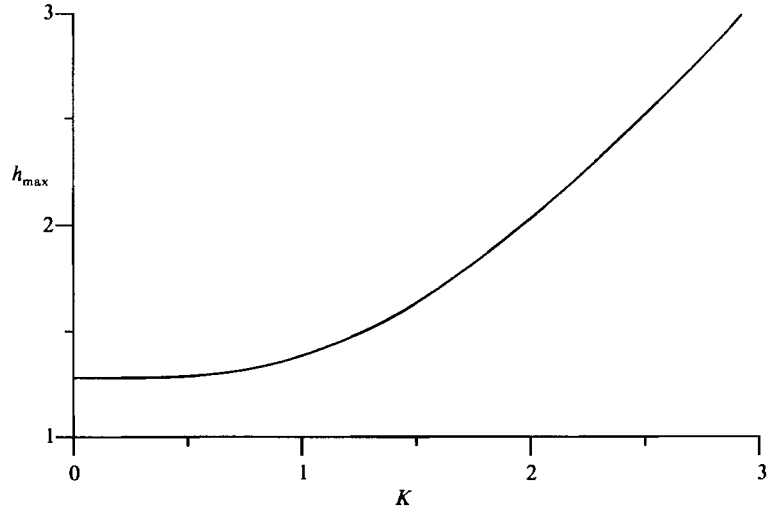

FIGURE 4. The variation of h_{max} with K for $x_0 = 0$.

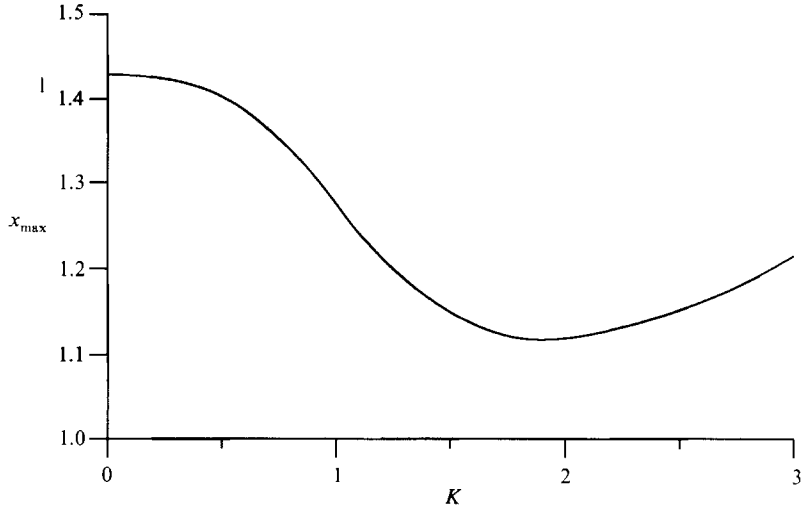

FIGURE 5. The variation of x_{max} with K for $x_0 = 0$.

The family of solutions found here all satisfy (2.10) and (2.12) and thus give $F = 0$ in the limit $M, N \to \infty$. Calculations show that for finite $N(< M)$ the contours of F form a valley in which $F \approx 0$ and which corresponds to the solutions above. We suggest, therefore, that the solution found by SST was simply the point in the valley for which the discretization error associated with a finite value of N was smallest. The solution should, instead, have been made unique by specifying K and imposing the boundary condition (2.13). We note that the values of h_{max} and x_{max} in our solution for $K = 1.84955$ agree with those calculated by SST.

We now consider solutions of (2.10)–(2.13) in which $x_0 > 0$. The changes in the shape of the crack as x_0 increases from zero are shown in figure 6 for $K = 1$ and $R = 2$. For $x_0 \leqslant 0.5$ the principal effect of the vapour in $x < x_0$ is to reduce the viscous pressures in the extreme tip of the crack and thus to reduce the elastic stress and the

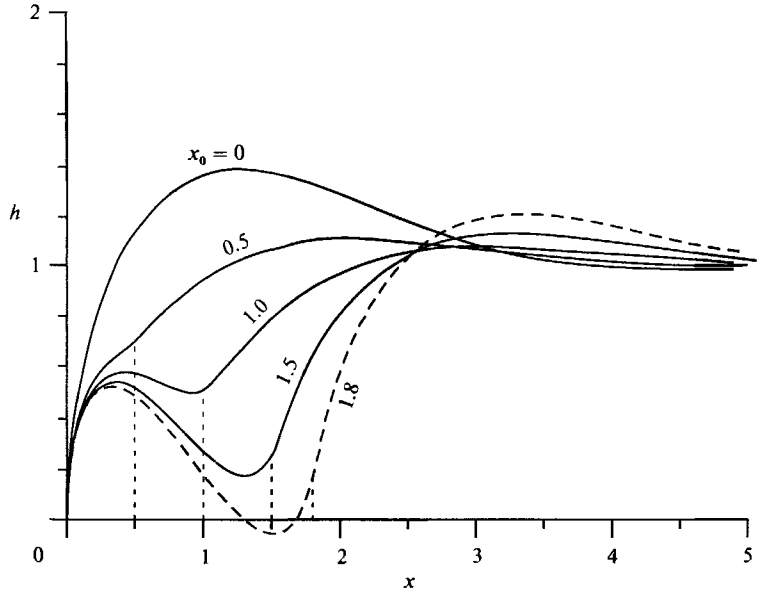

FIGURE 6. The variation of the shape of the crack with x_0 for $K = 1$ and $R = 2$. The solution for $x_0 = 1.8$ (dashed) is unphysical because there is a region where $h < 0$.

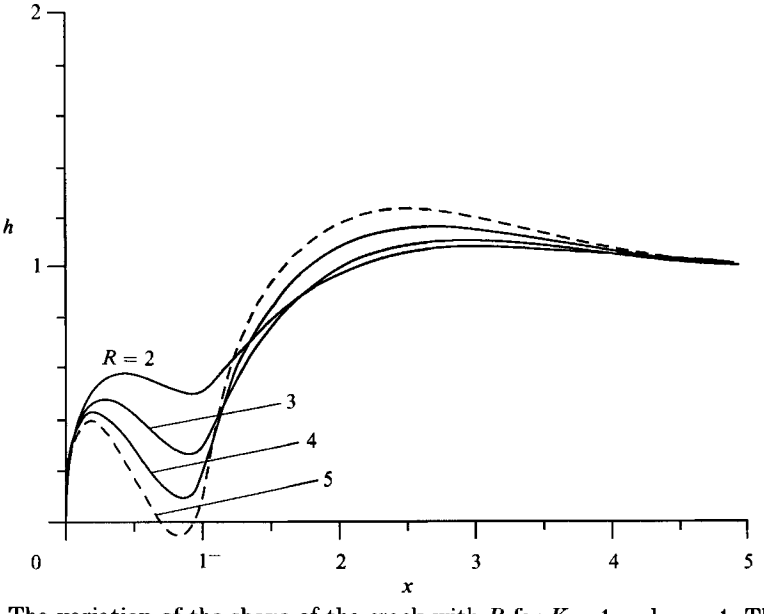

FIGURE 7. The variation of the shape of the crack with R for $K = 1$ and $x_0 = 1$. The solution for $R = 5$ (dashed) is unphysical because there is a region where $h < 0$.

size of the bulbous nose. For $x \geqslant 1$, however, the crack begins to neck-off near $x = x_0$. This necking-off is caused partly by the hydrostatic pressure gradient, which is greater in the vapour than in the liquid ($R > 1$), and partly by the low viscosity of the vapour, which cannot generate a viscous pressure gradient that would prevent the crack from closing. The influence of the hydrostatic pressure gradient may be seen in figure 7 which shows the increase in the tendency to neck-off as R increases with x_0 and K fixed.

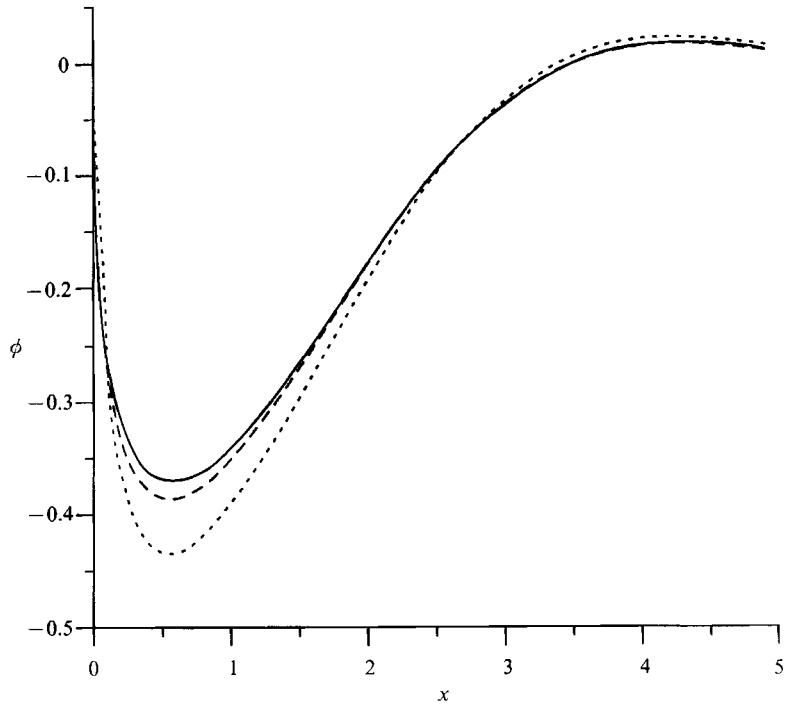

FIGURE 8. The solution ϕ (solid line) of the perturbation equations (3.2) for $K = 1$. Also shown are $(h(x;x_0)-h(x;0))/x_0^{\frac{1}{3}}$ for $x_0 = 0.025$ (dashed line) and $x_0 = 0.1$ (dotted line) with $K = 1$ and $R = 2$.

As x_0 increases further, a critical value x_0^* is attained beyond which h is negative in part of the region $0 < x < x_0$. It is found that $x_0^*(K,R)$ is an increasing function of K and a decreasing function of R, that $x_0^* > 0$ for all values of K and R and that $x_0^* \to 0$ as $R \to \infty$. In physical terms, the length of the column of vapour that can be supported by the medium increases as the strength of the medium increases or the buoyancy of the vapour decreases, is always greater than zero but becomes very small if the buoyancy of the vapour is very large. A useful qualitative comparison may be made with a finite, stationary crack lying in $0 < x < x_0$ and in which there is a linear hydrostatic pressure $p = P_0 - Rx$. The width of the crack is given by $h = (x(x_0-x))^{\frac{1}{2}}(P_0 - \frac{1}{2}Rx - \frac{1}{4}Rx_0)$ (Erdelyi *et al.* 1954, pp. 246–248, equations 19, 21, 25). If the stress intensity at $x = 0$ does not exceed K (i.e. $P_0 - \frac{1}{4}Rx_0 < K(2/x_0)^{\frac{1}{2}}$) then the crack will close at $x = x_0$ (i.e. $h < 0$) if $x_0 > 2(K/R)^{\frac{2}{3}}$ (cf. Weertman 1971; Pollard & Muller 1976).

Solutions for which $x_0 > x_0^*$ and $h < 0$ are clearly unphysical and we must examine our analysis of a propagating crack to see which assumptions have broken down in this regime. We note, first, that we have neglected the viscosity of the vapour by our use of (2.11) rather than an equation analogous to (2.10). If $x_0 > x_0^*$, however, this neglect is no longer valid since where h is sufficiently small the viscous pressures required to drive vapour though the narrow gap will ensure that the crack does not close completely. If the viscosity of the vapour is included in the model then solutions with large values of x_0 can be found which obey the physical constraint $h > 0$.

We note, secondly, however, that if x_0 is $O(1)$ then p_0 is also $O(1)$, corresponding to the propagation of the crack through the level at which the hydrostatic pressure in the solid is equal to the saturated vapour pressure in the liquid. In the absence of

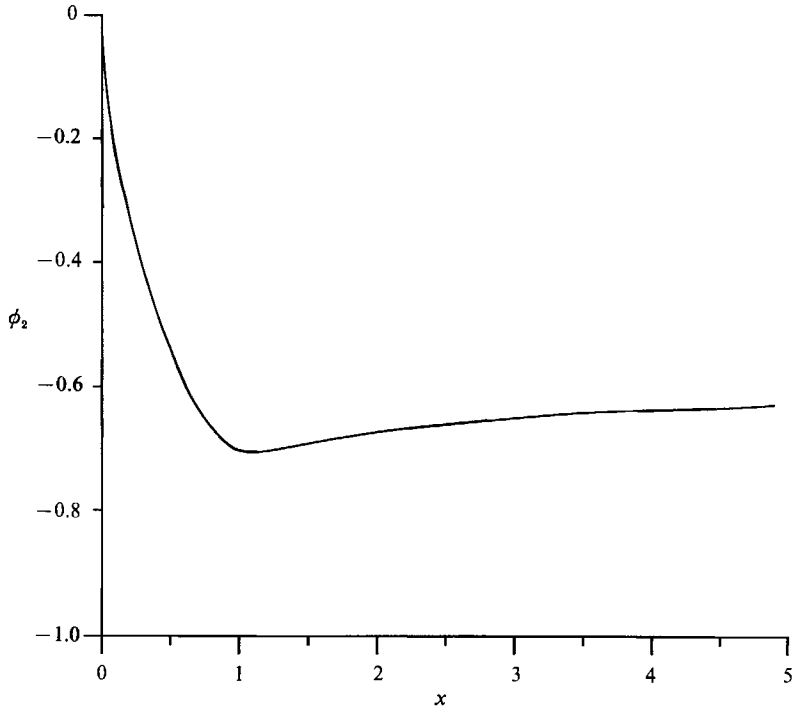

FIGURE 9. The solution ϕ_2 of the perturbation equations (3.3) for $K = 0$.

elastic stresses, liquid above this level would be supersaturated and, assuming the presence of nucleation sites, would exsolve vapour. As the crack propagates through this level, therefore, the required rate of vapour production from the liquid may be too large for the equilibrium between the vapour in the crack tip and the bulk liquid to be maintained and vapour bubbles are likely to be exsolved throughout the liquid. The subsequent upwards propagation of the vapour–liquid mixture is a problem of great geological interest and relates to volcanic eruptions of 'pyroclastic' material such as pumice; it is, however, beyond the scope of the present analysis.

Finally, we consider results from the limiting case $x_0 \ll 1, p_0 \gg 1$. In figure 8 we show the solution of the perturbation equations (3.2) for $K = 1$, together with the difference between the solutions of (2.10)–(2.13) for $x_0 = 0$ and some small values of x_0. The good agreement between the curves as $x_0 \to 0$ provides a useful check on both the numerical scheme and the perturbation analysis. In figure 9 we show the solution of the perturbation equations (3.3) for $K = 0$. We find that $\phi_1(1) = -0.0547\ldots$, $\phi_2(1) = -0.704\ldots$ and $\psi(1) = -4.046\ldots$. We deduce that $p_0 \sim -1.792 x_0^{-\frac{1}{3}}$ and $h(x_0) \sim 0.694 x_0^{\frac{2}{3}}$ as $x_0 \to 0$. The calculated values of p_0 and $h(x_0)$ are plotted against x_0 in figures 10 and 11. The agreement with the asymptotic values confirms the validity of (3.4) and (3.5).

6. Discussion

Our analysis of a buoyancy-driven fluid fracture has revealed a number of new physical phenomena. Confining attention, first, to the solutions in which no vapour is present, we have found a family of solutions parameterized by the non-dimensional

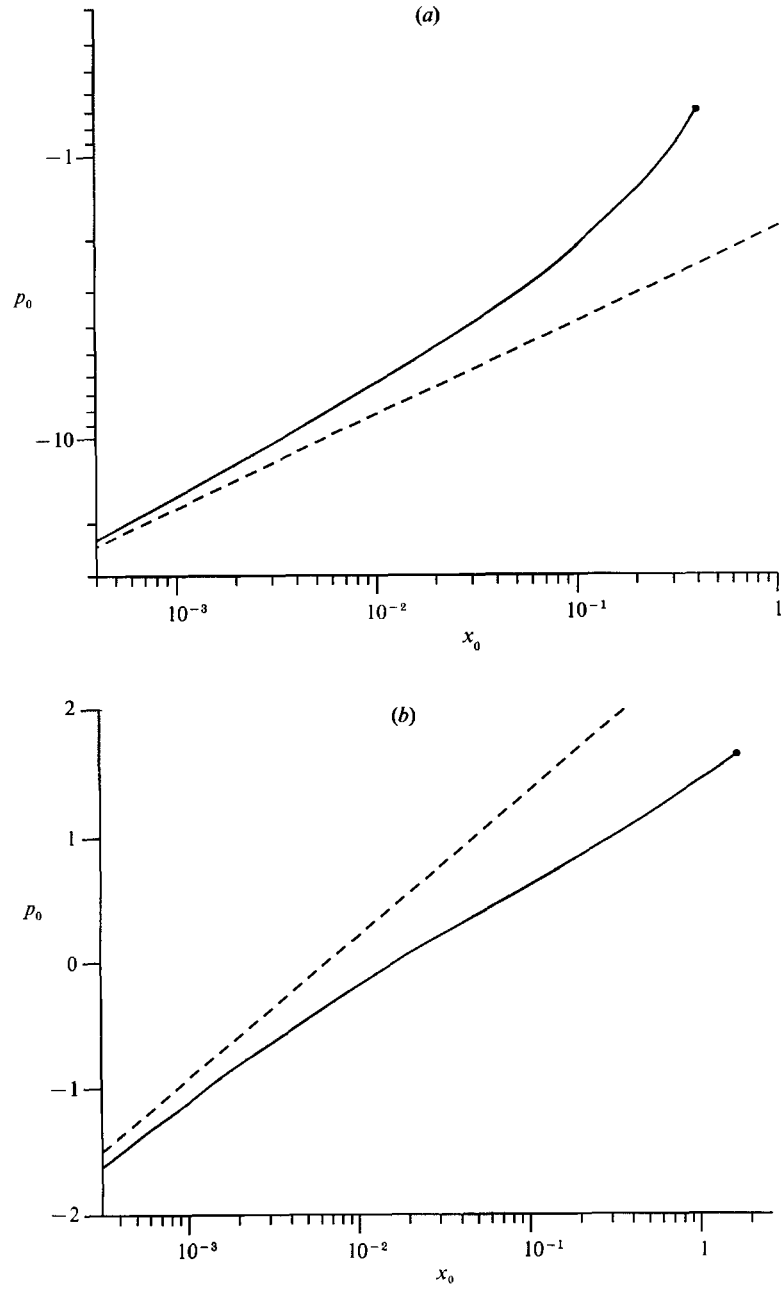

FIGURE 10. The variation of p_0 with x_0 for $R = 2$ (solid lines). The solution curves are terminated at the critical value x_0^* at which h first becomes negative. (*a*) $K = 0$ with asymptotic solution $p_0 \sim -1.792 x_0^{-\frac{1}{3}}$ (dashed line). (*b*) $K = 1$ with asymptotic solution $p_0 \sim \frac{1}{2}\ln x_0 + 2.50$ (dashed line).

stress intensity of the medium. Each member of this family has the same asymptotic width, which is prescribed by the flow rate into the base of the crack and is independent of the strength of the medium. The conclusion follows that the width and rate of propagation of the crack are determined by the fluid mechanics at depth and, in particular, by the geometry of the source reservoir feeding the crack and the

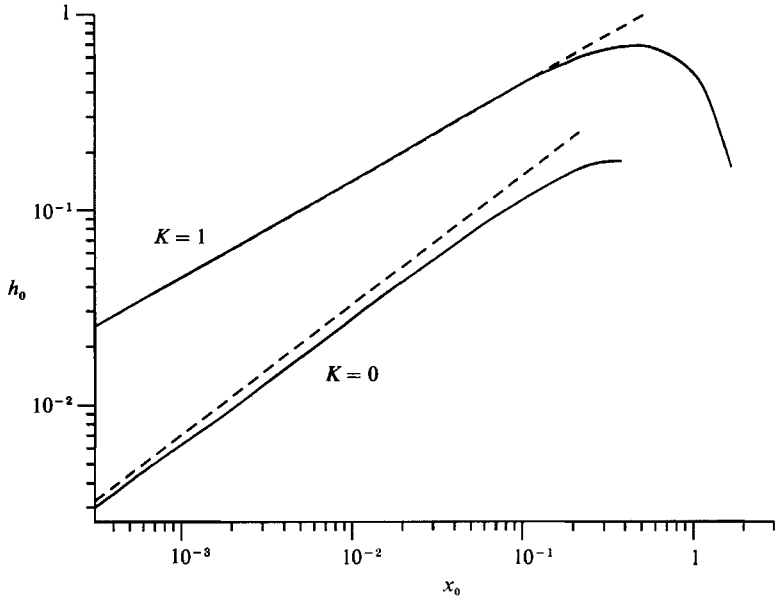

FIGURE 11. The variation of $h_0 \equiv h(x_0)$ with x_0 for $R = 2$ (solid lines). The asymptotic solutions are $h_0 \sim 0.694 x_0^{\frac{2}{3}}$ for $K = 0$ and $h_0 \sim (2x_0)^{\frac{1}{2}}$ for $K = 1$ (dashed lines).

supply rate that the reservoir can sustain. The properties of the medium affect only the structure near the tip of the crack. This picture is quite different from that deduced from the results of SST who, having found only one solution, deduced that a steadily propagating crack has a width and propagation rate which are determined by the strength of the medium.

The solutions in which the crack is entirely filled with liquid exhibit a region of large negative pressures near the tip of the crack. This feature will be present near the crack tip in all solutions representing the extension of a liquid-filled crack (e.g. Spence & Sharp 1985) and corresponds to the large pressure gradients required to drive a viscous liquid into a narrow gap. We argue that vapour will be exsolved from the liquid under such low pressures and, consequently, that the presence of relatively inviscid volatiles will be a general phenomenon in the tips of extending cracks.

A complementary observation to the above is that it is difficult for a liquid-filled crack to close completely since large elastic pressures are required to squeeze fluid out of a thin gap. This will be particularly relevant in geophysical applications since magmatic viscosities are large. The resistance to closure is a *dynamical* effect. We conclude that models of the transport of magma (e.g. Weertman 1971; Maaloe 1987) which are based on elasticity theory and fluid *statics* can be quite misleading. In particular, we suggest that the cessation of flow in a dyke is more likely to be related to a fall in pressure in the source reservoir and subsequent solidification of the slower flow than to the maximum volume of a hydrostatically pressurized crack.

It is of some interest to apply our solutions for a propagating crack to the ascent of magma through the Earth's lithosphere. (A more detailed discussion of this application may be found in Lister 1989.) We take as typical values $G = 2 \times 10^{10}$ Pa (Griggs, Turner & Heard 1960), $\nu = 0.25$, $\rho_1 = 2600$ kg m^{-3}, $\mu = 100$ Pa s (Rubin & Pollard 1987), $\Delta\rho = 300$ kg m^{-3} (SST), $g = 10$ m s^{-2} (Dziewonski, Hales & Lapwood 1975) and $K = 4 \times 10^6$ Pa m$^{\frac{1}{2}}$ (Atkinson 1984) and suppose that the crack has width

$2h_\infty = 1$ m. We find that $Q = 2.5\ \mathrm{m^2\ s^{-1}}$ and $c = 2.5\ \mathrm{m\ s^{-1}}$, which are in reasonable agreement with geological observations, and that the Reynolds number $\rho_l c h_\infty/\mu$ is 35 and within the laminar regime. From (2.7) we find that $\hat{x} \approx 2.1$ km, $\hat{p} \approx 6\times10^6$ Pa and $\hat{K} \approx 3\times10^8\ \mathrm{Pa\ m^{\frac{1}{2}}}$. Thus $K \approx 7\times10^{-3} \ll 1$ and we make the approximation $K = 0$. If we assume that the nose of the dyke is 5 km below the level at which the melt is saturated with volatiles then $p_0 \approx -23$ and the dimensional value of x_0 is about 20 cm. As the dyke propagates towards the level at which the melt is saturated, the length of the vapour-filled tip increases and by the time the dyke is 500 m below the saturated level $p_0 \approx -2.3$ and $x_0 \approx 43$ m. Above this level, rapid extension of a necked-off, vapour-driven crack tip or vesiculation in the melt will occur and limit the applicability of the numerical calculation.

It is interesting to compare these calculations with those for a hotter and, consequently, less viscous melt. If μ is reduced to 2 Pa s and the flow rate is kept at $2.5\ \mathrm{m^2\ s^{-1}}$ then the crack width decreases to 30 cm, $\hat{x}$ to 1.1 km, $\hat{p}$ to 3×10^6 Pa and $\hat{K}$ to $10^8\ \mathrm{Pa\ m^{\frac{1}{2}}}$. The most significant effect of the decrease in the pressure scales associated with elastic deformation and viscous flow is that the size of the vapour-filled tip is reduced to 1.5 cm at 5 km and 5.2 m at 500 m below the level of saturation.

In conclusion, the analysis presented in this paper provides an approximate model for the ascent of magma through dykes in the Earth's lithosphere. It should be noted that, for simplicity, we have neglected the influence of temperature on the rheology of the melt and the effects, discussed by Bruce & Huppert (1989), of melting and solidification at the dyke walls. We have also neglected the interaction with the stress-free surface of the Earth and variations in the flux of melt from the mantle. The incorporation of these and other effects into more complex models will provide challenges in the future for both fluid-dynamicists and geophysicists.

I am grateful to D. J. Stevenson, D. L. Turcotte and J. S. Turner for their useful comments and suggestions on an earlier version of this manuscript.

Appendix. Evaluation of integrals

The integral

$$I_\alpha(x;x_0) = \int_0^{x_0} \xi^\alpha k(\xi;x)\,\mathrm{d}\xi \equiv x_0^{\alpha+2}\int_0^1 \tau^\alpha k(\tau;t)\,\mathrm{d}\tau, \tag{A 1}$$

where $t = x/x_0$, arose in the calculation of Δh_1 in §3 for $\alpha = -\frac{4}{3}$ and -1 and in (4.5) for $\alpha = 0$. The case $\alpha = -1$ must be calculated numerically but is fortunately only needed for figure 2 since Δh_1 does not appear in (3.2). It is straightforward to calculate that

$$x_0^{-2} I_0 = -\tfrac{1}{2}(t-1)^2 \ln\left|\frac{t^{\frac{1}{2}}+1}{t^{\frac{1}{2}}-1}\right| + t^{\frac{1}{2}}(t-\tfrac{5}{3}). \tag{A 2}$$

The integral $I_{-\frac{1}{3}}$ may be integrated by parts twice, using $\partial^2 k/\partial\tau^2 = (t/\tau)^{\frac{1}{2}}/(\tau-t)$, to obtain

$$\tfrac{1}{3}x_0^{-\frac{2}{3}} I_{-\frac{4}{3}} = [(1-\tau^{-\frac{1}{3}})\,k]_0^1 + [\{(\tau-t)-\tfrac{3}{2}(\tau^{\frac{2}{3}}-t^{\frac{2}{3}})\}L]_0^1 + \int_0^1 \left(\frac{t}{\tau}\right)^{\frac{1}{2}}\left(1-\frac{3}{2}\frac{\tau^{\frac{2}{3}}-t^{\frac{2}{3}}}{\tau-t}\right)\mathrm{d}\tau, \tag{A 3}$$

where $L = \ln|(t^{\frac{1}{2}}+\tau^{\frac{1}{2}})/(t^{\frac{1}{2}}-\tau^{\frac{1}{2}})|$. The latter integral may be calculated by means of the substitution $\tau = t\theta^6$ to obtain

$$x_0^{-\frac{2}{3}} I_{-\frac{4}{3}} = 3\{(1-t)-\tfrac{3}{2}(1-t^{\frac{2}{3}})\}\ln\left|\frac{t^{\frac{1}{6}}+1}{t^{\frac{1}{6}}-1}\right| - 21t^{\frac{1}{6}} - \frac{27t^{\frac{2}{3}}}{4}\left(\ln\frac{c^2-c+1}{c^2+c-1} - \frac{2}{\sqrt{3}}\tan^{-1}\frac{\sqrt{3}c}{1-c^2}\right), \tag{A 4}$$

where $c = t^{-\frac{1}{6}}$ and the inverse tangent takes values in the interval $(0, \pi)$.

REFERENCES

Aki, K., Fehler, M. & Das, S. 1977 Source mechanisms of volcanic tremor: fluid-driven crack models and their application to the 1963 Kilauea eruption. *J. Volcanol. Geotherm. Res.* **2**, 259–287.

Anderson, O. L. 1978 The role of magma vapours in volcanic tremors and rapid eruptions. *Bull. Volcanol.* **41**, 341–353.

Anderson, O. L. & Grew, P. C. 1977 Stress corrosion theory of crack propagation with applications to geophysics. *Rev. Geophys. Space Phys.* **15**, 77–103.

Atkinson, B. K. 1984 Subcritical crack growth in geological materials. *J. Geophys. Res.* **89**, 4077–4114.

Barenblatt, G. I. 1962 The mathematical theory of equilibrium cracks in brittle fracture. *Adv. Appl. Mech.* **7**, 55–129.

Bruce, P. M. & Huppert, H. E. 1989 Solidification and melting in dykes by the laminar flow of basaltic magma. In *Magma Transport and Storage* (ed. M. P. Ryan). Wiley.

Carmichael, I. S. E., Nicholls, J., Spera, F. J., Wood, B. J. & Nelson, S. A. 1977 High temperature properties of silicate liquids: applications to the equilibration and ascent of basic magma. *Phil. Trans. R. Soc. Lond.* A **286**, 373–431.

Carslaw, H. S. 1930 *Introduction to the Theory of Fourier's Series and Integrals*. Dover.

Dziewonski, A. M., Hales, A. L. & Lapwood, E. R. 1975 Parametrically simple Earth models consistent with geophysical data. *Phys. Earth Planet. Inter.* **10**, 12–48.

Erdelyi, A., Magnus, W., Oberhettinger, F. & Tricomi, F. G. (eds.) 1954 *Tables of Integral Transforms*. McGraw Hill.

Griggs, D. T., Turner, F. J. & Heard, H. C. 1960 Deformation of rocks at 500 °C to 800 °C. In *Rock Deformation. Geol. Soc. Am. Mem.* **79**, 39–104.

Huppert, H. E., Sparks, R. S. J., Turner, J. S. & Arndt, N. T. 1984 Emplacement and cooling of komatiite lavas. *Nature* **309**, 19–22.

Irwin, G. R. 1958 Fracture. In *Handbuch der Physik VI* (ed. S. Flügge), pp. 551–590. Springer.

Lister, J. R. 1989 Fluid-mechanical models of crack propagation and their application to magma-transport in dykes. *Geophys. Res. Lett.* (in preparation).

Maaloe, S. 1987 The generation and shape of feeder dykes from mantle sources. *Contr. Min. Petrol.* **96**, 47–55.

Macdonald, R., Wilson, L., Thorpe, R. S. & Martin, A. 1988 Emplacement of the Cleveland Dyke: evidence from geochemistry, mineralogy and physical modelling. *J. Petrol.* **29**, 559–583.

Pollard, D. D. 1988 Elementary fracture mechanics applied to the structural interpretation of dykes. In *Mafic Dyke Swarms* (eds. H. C. Halls & W. H. Fahrig). Geol. Soc. Canada Special Paper 33.

Pollard, D. D. & Holzhausen, G. 1979 On the mechanical interaction between a fluid-filled fracture and the Earth's surface. *Tectonophysics* **53**, 27–57.

Pollard, D. D. & Muller, O. H. 1976 The effects of gradients in regional stress and magma pressure on the form of sheet intrusions in cross-section. *J. Geophys. Res.* **91**, 975–984.

Reches, Z. & Fink, J. 1988 The mechanism of intrusion of the Inyo Dike, Long Valley Caldera, California. *J. Geophys. Res.* **93**, 4321–4334.

Rubin, A. M. & Pollard, D. D. 1987 Origins of blade-like dikes in volcanic rift zones. *US Geol. Surv. Professional Paper* 1350.

SHAW, H. R. 1980 The fracture mechanisms of magma transport from the mantle to the surface. In *Physics of Magmatic Processes* (ed. R. B. Hargreaves), pp. 201–264. Princeton.

SPENCE, D. A. & SHARP, P. W. 1985 Self-similar solutions for elastohydrodynamic cavity flow. *Proc. R. Soc. Lond.* A **400**, 289–313.

SPENCE, D. A., SHARP, P. W. & TURCOTTE, D. L. 1987 Buoyancy-driven crack propagation: a mechanism for magma migration. *J. Fluid Mech.* **174**, 135–153 (referred to as SST).

SPERA, F. 1980 Aspects of magma transport. In *Physics of Magmatic Processes* (ed. R. B. Hargreaves), pp. 265–323. Princeton.

WEERTMAN, J. 1971 The theory of water-filled crevasses in glaciers applied to vertical magma transport beneath oceanic ridges. *J. Geophys. Res.* **76**, 1171–1183.